Preparation, Structure, and Luminescence of Dinuclear Lanthanide Complexes of a Novel Imine–Amine Phenolate Macrocycle

Karen D. Matthews and Ishenkumba A. Kahwa*

Chemistry Department, University of the West Indies, Mona, Kingston 7, Jamaica

David J. Williams

Chemistry Department, Imperial College of Science, Technology and Medicine, South Kensington, London SW7 2AY, United Kingdom

Received July 8, 1993®

Metal-free condensation of 2,6-diformyl-*p*-cresol with 3,6-dioxa-1,8-octanediamine followed by reduction with sodium tetrahydroborate and addition of lanthanide(III) nitrate salts, in that order, yield (slowly) crystalline dinuclear complexes of a novel imine–amine phenolate macrocycle **2**. The crystals of Ln_2**2**$(NO_3)_4 \cdot 1.2CH_3OH$ are monoclinic, space group $C2/c$; with Ln = Pr ($C_{31.2}H_{46.8}N_8O_{19.2}Pr_2$), a = 21.780(4) Å, b = 12.444(2) Å, c = 17.151(3) Å, β = 107.32(3)°, V = 4438 Å,^{3} and Z = 4. For 2282 observed data, R_w = 0.039 and R = 0.037. The decacoordination geometry of the identical Pr^{3+} ions is a C_{2v} 4A,6B-extended dodecahedron made up of two bidentate NO_3^- ions, two phenolate and two ether oxygens, and one imine and one amine nitrogens. Dinuclear lanthanide complexes of **2** appear to be more stable than those of the totally reduced chelate **3** in alcoholic media. The Tb_2**2**$(NO_3)_4 \cdot 1.2CH_3OH$ and $(La_{0.97}Tb_{0.03})_2$**2**$(NO_3)_4 \cdot 1.2CH_3OH$ compounds exhibit strong Tb^{3+} ($^5D_4 \rightarrow {}^7F_J$) emission sensitized by the singlet state of **2** at both 77 and 295 K. No Tb^{3+}–Tb^{3+} self-quenching or N–H trapping effects are observed at 77 K (decay rate is 598 s^{-1}); the coordination cavities of **2** are therefore potentially good hosts for Tb^{3+} in luminescent diagnostic agents. At room temperature the complex decay kinetics of Tb^{3+} in Tb_2**2**$(NO_3)_4 \cdot 1.2CH_3OH$ are similar to those of Tb_2**1**$(NO_3)_4 \cdot H_2O$ (*Chem. Abstr.* **1992**, *117*, 100045w). But for the dilute complex, $(La_{0.97}Tb_{0.03})_2$**2**$(NO_3)_4 \cdot 1.2CH_3OH$, unusual thermal equilibration of the ligand triplet and Tb^{3+} $^5D_4$ states occurs at room temperature; the ligand-to-Tb^{3+} energy-transfer rate is $\approx 4.36 \times 10^4$ s^{-1}, while Tb^{3+}-to-ligand back-energy-transfer is $\approx 7.1 \times 10^4$ s^{-1}.

Introduction

Contrary to a recent claim,[1] two structural reports on dinuclear lanthanide(III) (Ln^{3+}) complexes are available.[2-4] What is true, however, is that despite intense interest in the preparation, structure, and spectroscopy of this class of compounds, growing crystals of suitable quality for definitive X-ray analyses has been such a formidable task that only two macrocyclic ligands (both phenolates) have so far successfully yielded good crystals. Interestingly the formation of the series of dinuclear complexes via dimerization of mononuclear acyclic species is also facilitated by phenolate chelates.[1,5] Recently, an interesting series of dinuclear lanthanide compounds of a new neutral pyridine-type chelate were reported.[6] Although the strong circumstantial evidence given in support of dinuclearity is convincing, lack of crystallographic data underscores both the difficulties involved in studying molecular recognition processes leading to sequestration of a pair of Ln^{3+} cations and the need for more structural information on dinuclear Ln^{3+} systems where those difficulties have been overcome.

Dinuclear Ln^{3+} complexes are important as novel tunable photonic devices[7] with potential application in biomedical diagnostics[8] and fluorescence imaging[8,9] or paramagnetic contrast enhancing agents in magnetic resonance imaging.[10] The potential for heterodinuclear Ln^{3+} complexes to serve as atomically homogeneous precursors for oxides with well-defined electronic characteristics has been demonstrated.[11] Because of our interest in these phenomena and the development of efficient and selective extractive techniques for lanthanides in low-level sources, such as bauxite industrial waste, we have sought to understand the factors which influence Ln^{3+} dinucleation processes and subsequently prepare better dinucleating chelates. These studies are essential for development of critical design parameters and synthetic procedures for chelates of industrial potential.[12,13] Since molecular recognition processes are generally significantly influenced by small variations in the thermodynamic properties of the species involved,[14,15] we chose to modify systematically a previously characterized Schiff base complex series, Ln_2**1**$(NO_3)_4 \cdot H_2O$,[2,3] and study the nature of resulting complexes. The

* Abstract published in *Advance ACS Abstracts*, February 1, 1994.

(1) Liu, S.; Gelmini, L.; Rettig, S. J.; Thompson, R. C.; Orvig, C. *J. Am. Chem. Soc.* **1992**, *114*, 6081.
(2) Kahwa, I. A.; Folkes, S.; Williams, D. J.; Ley, S. V.; O'Mahoney, C. A.; McPherson, G. L. *J. Chem. Soc., Chem. Commun.* **1989**, 1531.
(3) Matthews, K. D.; Bailey-Folkes, S. A.; Kahwa, I. A.; McPherson G. L.; O'Mahoney, C. A.; Ley, S. V.; Williams, D. J.; Groombridge, C. J.; O'Connor, C. J. *J. Phys. Chem.* **1992**, *96*, 7021.
(4) Harrowfield, J. M.; Ogden, M. I.; White, A. H. *Aust. J. Chem.* **1991**, *44*, 1237, 1249. Bullita, E.; Cassellato, U.; Guerriero, P.; Vigato, P. A. *Inorg. Chim. Acta* **1987**, *139*, 59. Guerriero, P.; Vigato, P. A.; Fenton, D. E.; Hellier, P. C. *Acta Chem. Scand.* **1992**, *46*, 1025.
(5) Nelson, S. M. *J. Pure Appl. Chem.* **1980**, *52*, 2461.
(6) Ziessel, R.; Maestri, M.; Prodi, L.; Balzani, V.; Dorssedaer, A. V. *Inorg. Chem.* **1993**, *32*, 1237.
(7) Desvergne, J. P.; Fages, F.; Bouas-Laurent, H.; Marsau P. *Pure Appl. Chem.* **1992**, *64*, 1231.
(8) Balzani, V.; Ballardini, R. *Photochem. Photobiol.* **1990**, *52*, 409.
(9) Davidson, R. S.; Hilchenbach, M. M. *Photochem. Photobiol.* **1990**, *52*, 431.
(10) Lauffer, R. F. *Chem. Rev.* **1987**, *87*, 901.
(11) Kahwa, I. A.; Selbin, J.; Hsieh, T. C.-Y.; Evans, D. W.; Pamidimukkala, K. M.; Laine, R. A. *Inorg. Chim. Acta* **1988**, *141*, 131. Cassellato, U.; Guerriero, P.; Tamburini, S.; Sitran, S.; Vigato, P. A. *J. Chem. Soc., Dalton Trans.* **1991**, 2141.
(12) Schneider, H.-J. *Angew. Chem., Int. Ed. Engl.* **1991**, *30*, 1417.
(13) Izatt, R. M.; Christensen, J. J. *Synthesis of Macromolecules. The Design of Selective Complexing Agents*; Wiley Int. Sci.: New York, 1987.
(14) Izatt, R. M.; Eatough, D. J.; Christensen, J. J. *Struct. Bonding (Berlin)* **1973**, *16*, 161.
(15) Izatt, R. M.; Bradshaw, J. J.; Nielson, S. A.; Lamb, J. D.; Christensen, J. J. *Chem. Rev.* **1985**, *85*, 271.

0020-1669/94/1333-1382$04.50/0

Scheme 1

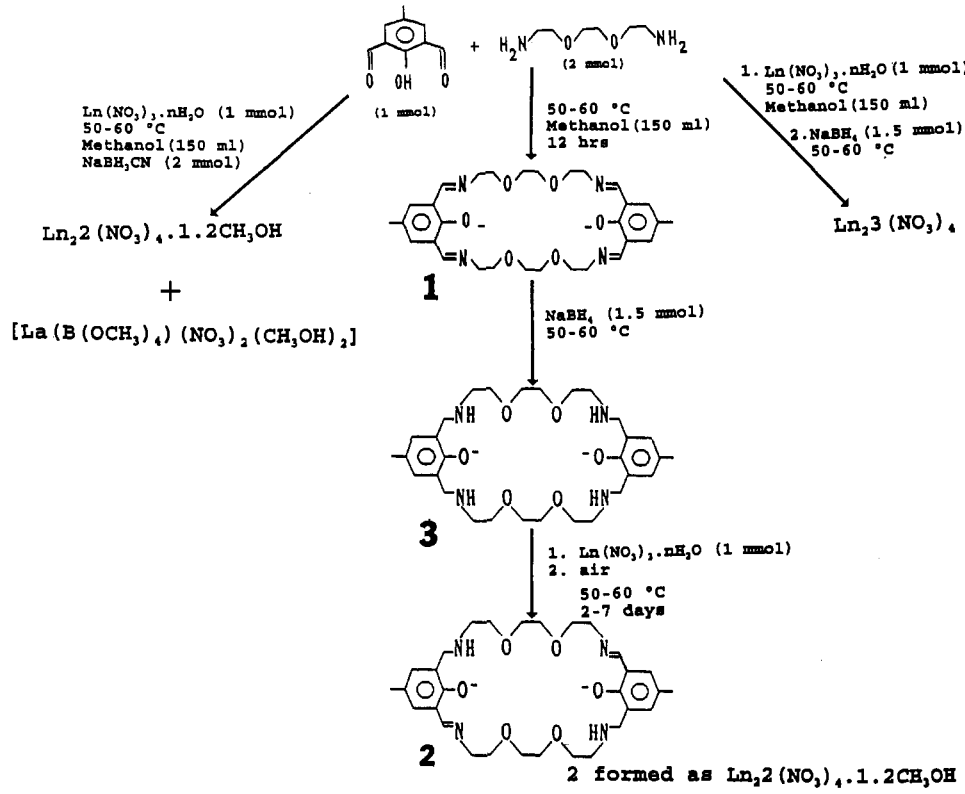

compounds $Ln_2\mathbf{1}(NO_3)_4{\cdot}H_2O$, which are obtained readily by a template procedure in high yield, were subjected to reduction protocols with sodium cyanohydroborate and sodium tetrahydroborate in an effort to prepare complexes of imine–amine intermediates such as **2** and eventually the amine phenolate **3**. Complexes of intermediates, like **2**, are important because they combine desirable characteristics of N–H groups which could be converted to better Ln^{3+} binding alkylamino derivatives, such as N–R, R = CH_2COO^- or CH_2CH_2OH, with efficient ligand-to-Ln^{3+} energy-donor properties of imine–phenolate groups.[3] Chelate **3** is important because of the diverse variety of ligands that are potentially accessible via alkylation of the N–H sites.[16] The complex reductive amination process of 2,6-diformyl-*p*-cresol with 3,6-dioxa-1,8-octanediamine in which compounds of $B(OCH_3)_4^-$, **2**, and **3** are formed was described earlier.[17]

Herein we report a one-pot synthetic procedure, the molecular structure, and the luminescence characteristics of a new series of dinuclear $Ln_2\mathbf{2}(NO_3)_4{\cdot}1.2CH_3OH$ complexes, which appear to be more stable than those of **3** and are strong phosphors when Ln = Tb.

Experimental Section

Materials. 2,6-Diformyl-*p*-cresol was prepared using a literature method,[18] while 3,6-dioxa-1,8-octanediamine was a gift from Texaco Chemicals Co. The lanthanide(III) nitrates were obtained from 99.9% lanthanide oxides from Aldrich Chemical Co. except for Eu^{3+} and Tb^{3+} complexes, where 99.99% pure oxides were employed. Sodium cyanotrihydroborate (95%) and sodium tetrahydroborate (98%) were supplied by Aldrich.

Elemental Analyses. Carbon, hydrogen, and nitrogen analyses were performed by Medac Ltd., Brunel University, Uxbridge, U.K. Lanthanide concentrations were obtained by nuclear activation analysis using the Slowpoke-II reactor at the Center for Nuclear Sciences, University of the West Indies, Kingston, Jamaica, and were comparable to those obtained by inductively coupled plasma methods (Galbraith, Knoxville, TN).

Spectroscopic Studies. The Perkin-Elmer FT-IR instrument and procedures used for cross polarization magic angle spinning (CP-MAS) ^{13}C NMR (300 MHz), the Perkin-Elmer LS5 luminescence spectrometer, and the PT2300 nitrogen and dye laser with its electronic support and homemade computational programs[19] were described previously.

Preparations. (a) $Ln_2\mathbf{2}(NO_3)_4{\cdot}1.2CH_3OH$ via Metal -Free Condensation of 1. $Ln_2\mathbf{2}(NO_3)_4{\cdot}1.2CH_3OH$ (Ln = La, Pr, Nd, Eu, Tb) complexes were prepared by a series of reactions described in Scheme 1. The presence of **1** in the initial condensation step was confirmed by the formation of familiar $Ln_2\mathbf{1}(NO_3)_4{\cdot}H_2O$ when $Ln(NO_3)_3{\cdot}nH_2O$ salts were added to the metal-free condensation product in methanol. Crystals of $Ln_2\mathbf{2}(NO_3)_4{\cdot}1.2CH_3OH$ were tabular parallelopipeda suitable for X-ray analyses. The colors and yields were as follows: Ln = La, nearly colorless (20%); Pr, light green (20%); Nd, violet (≈2%); Tb, yellow (20%). Anal. Calcd for $La_2\mathbf{2}(NO_3)_4{\cdot}1.2CH_3OH$: C, 33.5; H, 4.22; N, 10.02. Found: C, 33.18; H, 4.30; N, 9.68. Calcd for $Tb_2\mathbf{2}(NO_3)_4{\cdot}1.2CH_3OH$: C, 32.48; H, 4.09; N, 9.71. Found: C, 32.20; H, 3.81; N, 9.49.

The mixed lanthanum–terbium and lanthanum–europium samples were prepared in a similar procedure with the La:Tb and La:Eu ratios in the reaction mixtures being 8:2 and 9:1, respectively. Analysis of the samples by neutron activation analysis (NAA) gave 21.4% (La) and 0.8% (Tb), which correspond to approximately $(La_{0.97}Tb_{0.03})_2\mathbf{2}(NO_3)_4{\cdot}1.2CH_3OH$, and 21.2% (La) and 2.7% (Eu), which gives the stoichiometry $(La_{0.89}Eu_{0.11})_2\mathbf{2}(NO_3)_4{\cdot}1.2CH_3OH$.

^{13}C CP-MAS NMR (300 MHz, standard external $SiMe_4$) for diamagnetic $La_2\mathbf{2}(NO_3)_4{\cdot}1.2CH_3OH$: δ 20.6 (aromatic CH_3), 48.2 ($NH–CH_2$), 50.3 (methanolic CH_3), (CH_2O), 127.4 (non-phenolic aromatic quaternary), 135.2 (aromatic nonquaternary on the amine side of **2**), 158.5 (phenolic), and 168.0 (imine).[2,3]

(16) Alcock, N. W.; Kingston R. G.; Moore, P.; Pierpoint C. *J. Chem. Soc., Dalton Trans.* **1984**, 1937 and references therein.
(17) Matthews, K. D.; Kahwa, I. A.; Johnson, M.; Mague, J. T.; McPherson, G. L. *Inorg. Chem.* **1993**, *32*, 1442.
(18) Harfenist, M.; Bailey, A.; Lazier, W. A. *J. Org. Chem.* **1954**, 1608.
(19) Matthews, K. D.; Fairman, R. A.; Johnson, A.; Spence, K. V. N.; Kahwa, I. A.; McPherson, G. L.; Robotham, H. *J. Chem. Soc., Dalton Trans.* **1993**, 1719.

Table 1. Crystallographic Data for the Pr_2**2**$(NO_3)_4 \cdot 1.2CH_3OH$ Complex

formula	$C_{31.2}H_{46.8}N_8O_{19.2}Pr_2$
T, K	293
radiation, λ, Å	Cu Kα; 1.541 78
fw	1123
cryst system	monoclinic
space group	$C2/c$
a, Å	21.780(4)
b, Å	12.444(2)
c, Å	17.151(3)
β, deg	107.32(3)
V, Å^3	4438(1)
Z	4
D_{obs}/D_{calc}, g·cm^{-3}	1.73/1.68
μ, cm^{-1}	173.48
no. of unique data	3087
no. of obsd data ($I \geq 3\sigma(I)$)	2282
final shift/esd in final cycle	0.09
no. of variables	282
R^a	0.037
$R_w{}^b$	0.039
GOF^c	1.57

^{a} $R = \sum||F_o| - |F_c||/\sum F_o$. ^{b} $R_w = [\sum w(|F_o| - |F_c|)^2/\sum w(F_o)^2]^{1/2}$ with $w^{-1} = \sigma^2(F) + 0.0005F^2$. ^{c} GOF $= [\sum w(|F_o| - |F_c|)^2/(N_o - N_v)]^{1/2}$, where N_o and N_v are respectively the number of observations and variables.

Although the above synthetic procedure worked well most of the time, there are a few times when, unexpectedly, the crystals were not obtained or took well over 1 week to be deposited in the 250-mL conical flasks used. Addition of one or two drops of ≈0.5 M HNO_3 was in such cases helpful and was essential for the formation of the terbium complex (Tb_2**2**$(NO_3)_4 \cdot 1.2CH_3OH$).

(b) $Ln_2$3$(NO_3)_4$. A methanolic mixture of 2,6-diformyl-*p*-cresol (1 mmol), $Ln(NO_3)_3$ (1 mmol), and 3,6-dioxa-1,8-octanediamine (2 mmol) was heated at 50–60 °C until deposition of crystals of Ln_2**1**$(NO_3)_4 \cdot H_2O$ had begun. An excess of sodium cyanoborohydride was then added, and the reaction was allowed to proceed to completion. The solid complexes deposited have a needlelike morphology and are off-white for Ln = La, light green for Ln = Pr, and violet for Ln = Nd; the yields of the crude products were approximately 20%, 20%, and 15%, respectively.

Analyses (samples were carefully selected on the microscope to ensure that crystals of one phase were being analyzed in all cases) are as follows. Anal. Calcd for La_2**3**$(NO_3)_4$: C, 33.22; H, 4.28; N, 10.33. Found: C, 33.43; H, 4.18; N, 10.16. Calcd for Pr_2**3**$(NO_3)_4$: C, 33.10; H, 4.26; N, 10.30. Found: C, 33.02; H, 4.20; N, 9.81. Calcd for Nd_2**3**$(NO_3)_4$: C, 32.90; H, 4.23; N, 10.23. Found: C, 33.07; H, 4.22; N, 9.83.

Crystal Structure Determination. The essential experimental conditions for the crystal structure determination and resulting crystal data are summarized in Table 1; other details are available as supplementary material. A pale green tabular parallelopipeda crystal (0.13 × 0.23 × 0.27 mm^3) of Pr_2**2**$(NO_3)_4 \cdot 1.2CH_3OH$, obtained from the above preparation, was mounted on a Nicolet R3m diffractometer with graphite-monochromatized Cu Kα radiation using ω-scans. The structure was solved by the heavy-atom method and refined (full-matrix least-squares) anisotropically using absorption-corrected data (face-indexed numerical, maximum and minimum transmission factors 0.194 and 0.059) to give $R = 0.037$ and $R_w = 0.039$ for 2282 independent observed reflections [$|F_o| > 3\sigma(|F_o|)$; $\theta < 58°$]. The positions of the hydrogen atoms were idealized with C–H distances constrained to 0.95 Å, assigned isotropic thermal parameters, and allowed to ride on their parent carbon atoms. All computations were carried out on an IBM Model 70 386 PC using the SHELXTL PC program system.[20] Atomic coordinates are given in Table 2. Additional crystallographic data are provided as supplementary material.

(20) Sheldrick, G. M. SHELXTL PC version 4.2, Siemens Analytical X-ray Instruments Inc., 1990.

Table 2. Positional Parameters and U_{eq} Values (Å^2 × 10^3) with Esd's in Parentheses for La_2**2**$(NO_3)_4 \cdot 1.2CH_3OH$

	x	y	z	$U_{eq}{}^a$
Pr(1)	0.4028(1)	0.2501(1)	0.2189(1)	34(1)
C(1)	0.4458(4)	0.4560(6)	0.0922(5)	61(4)
N(2)	0.3940(3)	0.4305(5)	0.1280(4)	42(2)
C(3)	0.3306(4)	0.4380(8)	0.0677(5)	69(4)
C(4)	0.2792(4)	0.4257(7)	0.1050(5)	58(3)
O(5)	0.2869(2)	0.3301(4)	0.1532(3)	53(2)
C(6)	0.2369(4)	0.2546(7)	0.1243(7)	75(4)
C(7)	0.2412(4)	0.1706(8)	0.1848(7)	83(5)
O(8)	0.3040(2)	0.1207(4)	0.2056(3)	58(2)
C(9)	0.3104(4)	0.0383(7)	0.2673(6)	76(4)
C(10)	0.3789(4)	−0.0003(6)	0.2949(5)	65(4)
N(11)	0.4207(3)	0.0924(5)	0.3233(4)	55(3)
C(12)	0.4460(4)	0.0970(6)	0.3997(5)	53(3)
C(13)	0.4837(3)	0.1890(6)	0.4446(4)	45(3)
C(14)	0.4961(4)	0.1953(8)	0.5304(5)	64(4)
C(15)	0.5282(5)	0.2810(8)	0.5759(5)	65(4)
C(16)	0.5472(4)	0.3644(7)	0.5351(4)	53(3)
C(17)	0.5368(3)	0.3616(5)	0.4518(4)	41(3)
C(18)	0.5067(3)	0.2735(5)	0.4052(4)	38(3)
O(18)	0.5004(2)	0.2704(3)	0.3249(3)	37(2)
C(19)	0.5395(7)	0.2828(9)	0.6676(6)	108(6)
N(10)	0.3573(3)	0.3846(5)	0.3414(4)	51(3)
O(11)	0.3490(3)	0.2846(5)	0.3337(3)	56(2)
O(12)	0.3873(3)	0.4288(4)	0.2980(3)	55(2)
O(13)	0.3370(3)	0.4352(5)	0.3889(4)	82(3)
N(20)	0.3836(3)	0.0923(5)	0.0795(4)	51(3)
O(21)	0.3578(2)	0.1847(4)	0.0701(3)	50(2)
O(22)	0.4204(3)	0.0708(4)	0.1500(3)	54(2)
O(23)	0.3745(3)	0.0295(5)	0.0226(4)	77(3)
O(50)	0.2091(22)	0.2120(20)	0.3814(17)	325(30)
C(50)	0.1734(23)	0.2887(30)	0.3898(26)	212(27)

^{a} Equivalent isotropic U defined as one-third of the trace of the orthogonalized U_{ij} tensor.

Results and Discussion

Syntheses and Structural Data for $Ln_2$2$(NO_3)_4 \cdot 1.2CH_3OH$. The metal free reaction between 3,6-dioxa-1,8-octanediamine and 2,6-diformyl-*p*-cresol (Scheme 1) leads to the formation of chelate **1**. Reduction of metal-free **1** with a routine sodium tetrahydroborate protocol[21] is expected to yield the macrocyclic phenolate amine **3**.[16,22,23] However, when $Ln(NO_3)_3 \cdot nH_2O$ salts are added to the methanolic reduction products, no solid complexes are deposited over 1 day and intractable products are obtained when the solvent is evaporated off. The nearly colorless methanolic solutions of the tetrahydroborate reduction products gradually become yellow and then orange before deposition of large crystals of Ln_2**2**$(NO_3)_4 \cdot 1.2CH_3OH$ begins. Without the $Ln(NO_3)_3 \cdot nH_2O$ salts the tetrahydroborate reduction solutions remain light yellow for a long time, but when the solvent is evaporated, IR spectra of the oils show absorption features due to the oxidation product >C=N–. Oxidation of the –CHNH– group to –C=N– is well-known for catalytic transition metal ions, but more drastic oxidizing conditions such as the use of peroxides or pressurized oxygen are usually needed.[24,25] Therefore, this template preparation of the asymmetric chelate **2** by selective oxidation of two of the four –HN–CH_2 groups of **3** in a simple one-pot procedure is a remarkably new result, the generality of which is being studied. These new results are important because a stepwise synthesis of an asymmetric and labile molecule such as **2** would definitely require several protection/deprotection cycles, which may be tedious and of low yield.

The formation of **2**, inferable from elemental analyses, is evidenced by characteristic IR absorptions of the –C=N– (1620

(21) Borch, R. F. *Org. Synth.* **1972**, *52*, 124.
(22) Chen, D.; Martell, A. *Tetrahedron* **1991**, *47*, 6895.
(23) Mandal, S. K.; Thompson, L. K.; Nag, K.; Charland, J.-P.; Gabe, E. J. *Inorg. Chem.* **1987**, *26*, 1391.
(24) Murahashi, S.-I.; Naota, T.; Taki, H. *J. Chem. Soc., Chem. Commun.* **1985**, 613.
(25) Nishinaga, A.; Yamazaki, S.; Matsuura, T. *Tetrahedron Lett.* **1988**, *29*, 4115.

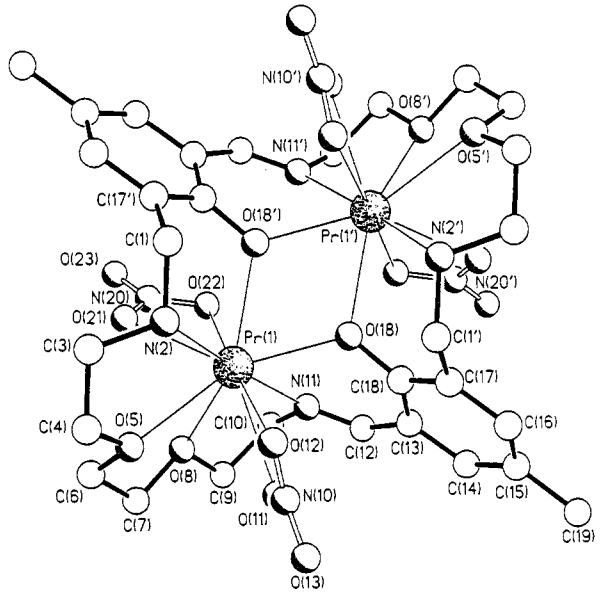

Figure 1. Molecular structure of Pr_2**2**$(NO_3)_4 \cdot 1.2CH_3OH$.

cm^{-1}) and >N–H (3200 cm^{-1}) groups[17] and by the ^{13}C CP-MAS NMR spectrum of the La_2**2**$(NO_3)_4 \cdot 1.2CH_3OH$ complex, which shows –C=N– (168.95 ppm) and –CH–NH– (48.20 ppm). The most convincing evidence is the crystal structure of the Pr_2**2**$(NO_3)_4 \cdot 1.2CH_3OH$ complex, which reveals entrapment of a pair of Pr^{3+} cations in the twin 18-membered coordination cavities of the compartmental chelate **2** (Figure 1) and two sets of trans carbon–nitrogen linkages corresponding to –CH=N– (1.263(10) Å) and $-CH_2-NH-$ (1.471(12) Å) (Table 3).

The molecular structure of the Pr_2**2**$(NO_3)_4 \cdot 1.2CH_3OH$ complex shows a geometry very similar to that of the Gd_2**1**$(NO_3)_4 \cdot H_2O$ complex.[2] Reduction of **1** to **3**, followed by an *in situ* oxidation to **2**, results in a lowering of the molecular D_2 symmetry exhibited by Gd_2**1**$(NO_3)_4 \cdot H_2O$ to C_2 for Pr_2**2**$(NO_3)_4 \cdot 1.2CH_3OH$. The 2-fold axis passes through the center of, and is perpendicular to, the plane formed by the Pr^{3+} cations and their bridging phenolic oxygen atoms. The reduction in molecular symmetry is due to a change in the conformation of the macrocycle, the single C(1)–N(2) bond being rotated ca. 67° out of the plane of its associated aromatic ring, whereas the N(11)–C(12) double bond retains coplanarity with this ring. In the Gd_2**1**$(NO_3)_4 \cdot H_2O$ complex[2] both of these bonds are essentially coplanar with their corresponding aromatic rings. The aromatic rings are inclined by ca. 62° in opposite senses relative to the Pr_2O_2 mean plane. The Pr_2O_2 ring is slightly folded (by ca. 14°) about the O(18)–O(18′) direction. The Pr–Pr and O(18)–O(18′) distances, 4.05 and 2.56 Å, respectively, are comparable to those found in other complexes containing Ln_2O_2 rings.[1-4] The Pr–O–Pr′ bridges are asymmetric with Pr–O(18) and Pr–O(18′) distances being 2.363(4) and 2.454(5) Å, respectively. The transannular distances however are comparable to those found in Gd_2**1**$(NO_3)_4 \cdot H_2O$.[2]

Each Pr^{3+} cation is ten coordinate, being bound by two bidentate nitrate anions, two phenolate oxygens, two ether oxygens, and one imine and one amine nitrogen atoms. The coordination distances (Table 3) are in the range 2.363–2.707 Å (for O(18) and N(2), respectively). In the typical behavior of strong Ln–O(phenolate) interactions,[26,27] the Pr–O(phenolate) bonds (2.363 and 2.453 Å) are the shortest of the ten contacts Pr^{3+} makes with other atoms. The coordination polyhedron (Figure 2) can best be described as a 4A,6B-extended dodecahedron of C_{2v} symmetry;[28,29] the 2-fold axis passes through the bisectors of O(5)–O(8) and O(18)–O(18′) edges. There is a possible weak intracomplex hydrogen bond (2.96 Å) between the amine nitrogen N(2) and one of the nitrate oxygens O(12). The methanol solvent molecules are not involved either in coordination to the Pr^{3+} centers or in hydrogen bonding to the complex. Other interatomic distances (Table 3) in the Pr_2**2**$(NO_3)_4 \cdot 1.2CH_3OH$ molecule are normal.[2,26]

The inability to obtain well-defined solid products of **3** (vide supra), immediately after the reduction step, suggests that the dinuclear complexes of **3** are unstable in alcoholic media. Since the complexes of **2** are later formed via an *in situ* oxidation process, we conclude qualitatively that $(Ln^{3+})_2$ interactions with **3** are not sufficient to overcome destabilizing repulsive Ln^{3+}–Ln^{3+} interactions as well as competing and stabilizing solvent effects (i.e. solvation enthalpy of the cavity of **3** and Ln^{3+}).[30] We can therefore conclude on the basis of this study that macrocyclic imines form more stable dinuclear Ln^{3+} complexes than corresponding amines. Consequently, chelate **1** yields Ln_2**1**$(NO_3)_4 \cdot H_2O$ readily for Ln = La–Dy and **2** forms Ln_2**2**$(NO_3)_4 \cdot 1.2CH_3OH$ with Ln = La–Nd (and with much greater effort (vide supra) Sm–Tb) in low yields. Complexes of **3** were sometimes obtained in templated

Table 3. Selected Bond Distances (Å) and Interbond Angles (deg) with Esd's in Parentheses

Pr(1)–N(2)	2.707(6)	Pr(1)–O(5)	2.634(5)
Pr(1)–O(8)	2.643(5)	Pr(1)–N(11)	2.606(6)
Pr(1)–O(18)	2.363(4)	Pr(1)–O(11)	2.608(6)
Pr(1)–O(12)	2.677(6)	Pr(1)–O(21)	2.578(5)
Pr(1)–O(22)	2.606(5)	Pr(1)–Pr(1′)	4.047(1)
Pr(1)-O(18′)	2.453(5)	C(1)–N(2)	1.471(12)
C(1)–C(17′)	1.505(11)	N(2)–C(3)	1.462(9)
C(3)–C(4)	1.454(14)	C(4)–O(5)	1.429(10)
O(5)–C(6)	1.411(10)	C(6)–C(7)	1.456(15)
C(7)–O(8)	1.445(10)	O(8)–C(9)	1.451(11)
C(9)–C(10)	1.502(12)	C(10)–N(11)	1.461(10)
N(11)–C(12)	1.263(10)	C(12)–C(13)	1.483(10)
C(13)–C(14)	1.418(11)	C(13)–C(18)	1.420(11)
C(14)–C(15)	1.381(13)	C(15)–C(16)	1.381(13)
C(15)–C(19)	1.519(13)	C(16)–C(17)	1.380(10)
C(17)–C(18)	1.399(9)	C(17)–C(1′)	1.505(11)
C(18)–O(18)	1.343(9)	O(18)–Pr(1′)	2.453(5)
N(10)–O(11)	1.258(9)	N(10)–O(12)	1.254(10)
N(10)–O(13)	1.212(10)	N(20)–O(21)	1.268(9)
N(20)–O(22)	1.265(8)	N(20)–O(23)	1.219(9)
O(50)–C(50)	1.266(59)		

N(2)–Pr(1)–O(5)	63.0(2)	N(2)–Pr(1)–O(8)	122.6(2)
O(5)–Pr(1)–O(8)	62.7(2)	N(2)–Pr(1)–N(11)	172.1(2)
O(5)–Pr(1)–N(11)	120.5(2)	O(8)–Pr(1)–N(11)	63.4(2)
N(2)–Pr(1)–O(18)	104.3(2)	O(5)–Pr(1)–O(18)	144.8(2)
O(8)–Pr(1)–O(18)	130.9(2)	N(11)–Pr(1)–O(18)	68.6(2)
N(2)–Pr(1)–O(11)	109.1(2)	O(5)–Pr(1)–O(11)	70.9(2)
O(8)–Pr(1)–O(11)	68.2(2)	N(11)–Pr(1)–O(11)	67.3(2)
O(18)–Pr(1)–O(11)	84.6(2)	N(2)–Pr(1)–O(12)	66.8(2)
O(5)–Pr(1)–O(12)	69.8(2)	O(8)–Pr(1)–O(12)	109.1(2)
N(11)–Pr(1)–O(12)	107.0(2)	O(18)–Pr(1)–O(12)	75.1(1)
O(11)–Pr(1)–O(12)	47.8(2)	N(2)–Pr(1)–O(21)	75.6(2)
O(5)–Pr(1)–O(21)	70.3(2)	O(8)–Pr(1)–O(21)	70.2(2)
N(11)–Pr(1)–O(21)	112.1(2)	O(18)–Pr(1)–O(21)	141.7(2)
O(11)–Pr(1)–O(21)	132.5(2)	O(12)–Pr(1)–O(21)	134.1(2)
N(2)–Pr(1)–O(22)	116.3(2)	O(5)–Pr(1)–O(22)	112.4(2)
O(8)–Pr(1)–O(22)	70.4(2)	N(11)–Pr(1)–O(22)	69.8(2)
O(18)–Pr(1)–O(22)	102.7(1)	O(11)–Pr(1)–O(22)	130.0(2)
O(12)–Pr(1)–O(22)	176.7(2)	O(21)–Pr(1)–O(22)	49.0(2)
N(2)–Pr(1)–Pr(1′)	92.3(1)	O(5)–Pr(1)–Pr(1′)	155.1(1)
O(8)–Pr(1)-Pr(1′)	141.6(1)	N(11)–Pr(1)–Pr(1′)	83.6(2)
O(18)–Pr(1)–Pr(1′)	33.5(1)	O(11)–Pr(1)–Pr(1′)	118.1(1)
O(12)–Pr(1)–Pr(1′)	98.4(1)	O(21)–Pr(1)–Pr(1′)	108.7(1)
O(22)–Pr(1)–Pr(1′)	80.5(1)	N(2)–Pr(1)–O(18′)	70.0(2)
O(5)–Pr(1)–O(18′)	129.2(2)	O(8)–Pr(1)–O(18′)	142.0(2)
N(11)–Pr(1)–O(18′)	108.7(2)	O(18)–Pr(1)–O(18′)	64.3(2)
O(11)–Pr(1)–O(18′)	146.5(1)	O(12)–Pr(1)–O(18′)	108.6(2)
O(21)–Pr(1)–O(18′)	80.6(2)	O(22)–Pr(1)–O(18′)	72.1(2)
Pr(1′)–Pr(1)–O(18′)	32.2(1)		

(26) Sofen, S. R.; Cooper, S. R.; Raymond, K. N. *Inorg. Chem.* **1979**, *18*, 1611.
(27) Hitchcock, P. B.; Lappert, M. F.; Singh, A. *J. Chem. Soc., Chem. Commun.* **1983**, 1499. Kahwa, I. A.; Fronczek, F. R.; Selbin, J. *Inorg. Chim. Acta* **1987**, *126*, 227.
(28) Sinha, S. P. *Struct. Bonding (Berlin)* **1974**, *25*, 69.
(29) Drew, M. G. B. *Coord. Chem. Rev.* **1977**, *24*, 179.
(30) Diederich, F.; Smithrud, D. B.; Sanford, E. M.; Wyman, T. B.; Ferguson, S. B.; Carcanaque, D. R.; Chao, I.; Houk, K. N. *Acta Chem. Scand.* **1992**, *46*, 205.

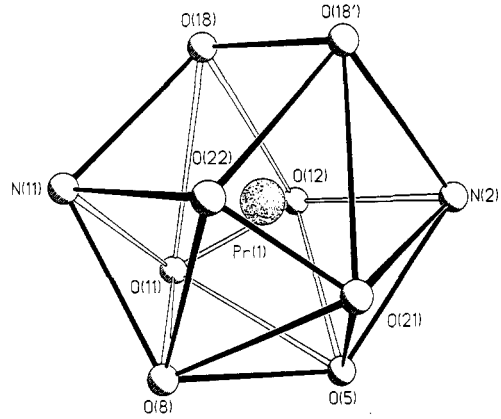

Figure 2. Perspective view of the 4A,6B-extended dodecahedral decacoordination geometry around the Pr^{3+} ions.

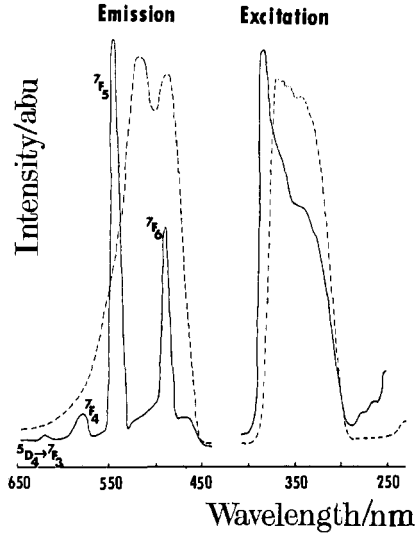

Figure 3. 77 K emission (excitation at 365 nm) and excitation [emission monitored at 500 nm for Ln = La (broken line) and 544 nm for Ln = La (97%) + Tb (3%) (solid line)] spectra of complexes of **2**.

reductive amination reactions (ref 17 and vide supra), but the exact requirements for this template formation are not understood.[17] Preparation of metal-free **3** by other routes is being undertaken to check these conclusions systematically, to establish the thermodynamics of the Ln^{3+}–**3** interactions, and to determine the factors influencing the oxidation of $-CH_2NH-$ to $-CH{=}N-$ functionalities.

The composition of the solid lanthanum–europium products resembles that of the mother reaction mixture, which shows that a lanthanide cation discrimination index[19] ≈1 applies. On the other hand, the lanthanum–terbium system reveals enrichment of La^{3+} from $La_{0.8}Tb_{0.2}$ in the reaction mixture to $La_{0.97}Tb_{0.03}$ in the crystalline product; hence, a higher lanthanide(III) cation discrimination index in favor of La^{3+} is observed. Although these results are inadequate for more definitive conclusions to be made about binding selectivity as for **1**,[19] it is clear, from the low yields of homodinuclear complexes of **2** with small Ln^{3+} (vide supra) and La^{3+} enrichment in $(La_{1-x}Tb_x)\mathbf{2}(NO_3)_4{\cdot}1.2CH_3OH$ at the expense of Tb^{3+}, that chelate **2** is a selective dinucleating agent.

Luminescence. Schiff Base Chelate. The absorption spectrum of the $La_2\mathbf{2}(NO_3)_4{\cdot}1.2CH_3OH$ compound features strong absorptions at about 278 and 364 nm typical of imine–phenolates.[3] The 77 K emission spectrum of the diamagnetic $La_2\mathbf{2}(NO_3)_4{\cdot}1.2CH_3OH$ complex (Figure 3) features phosphorescence with two maxima at 485 and 520 nm. The excitation spectrum of this intense phosphorescence shows strong singlet absorption centered at ≈350 nm (Figure 3). Thus, in sharp contrast to Schiff base **1**, the new imine–amine phenolate chromophore of **2** exhibits efficient intersystem crossing in the absence of paramagnetic ions. The emission and excitation spectra of **2** at 77 K are essentially similar to those obtained at 295 K, but 77 K emission is much more intense.

The luminescence decay kinetics of **2**, like those of **1**,[3] are very complicated; the decay curves are not exponential, and their profiles vary significantly with the emission monitoring wavelength. For example, with λ_{exc} = 337 nm and 77 K, the short lived emission of $La_2\mathbf{2}(NO_3)_4{\cdot}1.2CH_3OH$ at 460 nm decays at a rate $\approx 2.4 \times 10^3\ s^{-1}$ whereas the tail decays at $\approx 1.3 \times 10^2\ s^{-1}$. When monitored at 570 nm, the corresponding rates are $\approx 1.7 \times 10^3$ and $1.3 \times 10^2\ s^{-1}$, respectively. By contrast, chelate **1** in $La_2\mathbf{1}(NO_3)_4{\cdot}H_2O$ exhibits intense 77 K fluorescence[3] and a weak phosphorescence decaying at $\approx 7.0 \times 10^1\ s^{-1}$. There are at least two independent triplet states in **2** (Figure 3). Remarkable equilibration of some ligand and Tb^{3+} electronic states occur at room temperature (vide infra). Inspite of these complications chromophore **2** is an efficient sensitizer for intense Tb^{3+} emission. But **2** is inefficient for sensitization of emission from Eu^{3+}, which is very weak for both the dilute $(La_{0.9}Eu_{0.1})_2\mathbf{2}(NO_3)_4{\cdot}1.2CH_3OH$ and concentrated $Eu_2\mathbf{2}(NO_3)_4{\cdot}1.2CH_3OH$ samples presumably due to N–H quenching.

Tb^{3+} Emission at 77 K. Emission from both crystalline $Tb_2\mathbf{2}(NO_3)_4{\cdot}1.2CH_3OH$ and $(La_{0.97}Tb_{0.03})_2\mathbf{2}(NO_3)_4{\cdot}1.2CH_3OH$ is very intense at 77 K and is characteristic of Tb^{3+} ($^5D_4 \rightarrow {}^7F_J$) (Figure 3). The excitation spectrum for Tb^{3+} emission is dominated by singlet absorption of chelate **2**; a weak absorption feature due to Tb^{3+} ($^7F_6 \rightarrow {}^5D_4$) is also seen at ≈490 nm. When the sample is excited directly at 488 nm, the $^5D_4$ state decays exponentially at a rate of $6.0 \times 10^2\ s^{-1}$ at 77 K. But when the sample is excited at 337 or 365 nm via the singlet state of **2**, the decay curve of the dilute terbium sample shows weak excitation build up over ≈150 μs. This shows that some longer lived triplet state of **2** is also involved in sensitizing Tb^{3+} emission, albeit to a lesser extent compared to the singlet. This excitation buildup is the most convincing evidence for ligand-to-Tb^{3+} energy transfer; direct excitation of the $^5D_4$ level yields normal exponential decay kinetics for the Tb^{3+} emission with rate $\approx 6.0 \times 10^2\ s^{-1}$. The 77 K luminescence decay rates of Tb^{3+} in both the dilute and concentrated samples are similar ($6.0 \times 10^2\ s^{-1}$). No concentration quenching effects appear to be operative in $Tb_2\mathbf{2}(NO_3)_4{\cdot}1.2CH_3OH$ and since the Tb^{3+} in $Tb_2\mathbf{1}(NO_3)_4{\cdot}H_2O$ decays with a similar rate,[3] it is concluded that Tb^{3+} ($^5D_4$)-to-NH–quenching processes (chelate **2**) are inefficient at 77 K. These are favorable properties when considering **2** as a host for Tb^{3+} in biomedical luminescent diagnostics.

Thermal Equilibration of Ligand and Tb^{3+} ($^5D_4$) States at 295 K. The room-temperature luminescence decay behavior of Tb^{3+} in the dilute $(La_{0.97}Tb_{0.03})_2\mathbf{2}(NO_3)_4{\cdot}1.2CH_3OH$ complex is a most interesting revelation of Tb^{3+}-to-ligand (**2**) energy back-transfer;[31] essentially a near thermal equilibration of Tb^{3+} and ligand electronic states occurs. The room-temperature decay curve of Tb^{3+} emission is nonexponential (λ_{exc} = 488 nm into the $^5D_4$ level); in the early moments following excitation, the decay rate is seen to increase over 20-fold from $3.6 \times 10^3\ s^{-1}$ for the Tb–Tb homopair in $Tb_2\mathbf{2}(NO_3)_4{\cdot}1.2CH_3OH$ to $7.7 \times 10^4\ s^{-1}$ for the La–Tb heteropair in $(La_{0.97}Tb_{0.03})_2\mathbf{2}(NO_3)_4{\cdot}1.2CH_3OH$. The corresponding tails decay at $\approx 1.1 \times 10^3$ and $4.7 \times 10^3\ s^{-1}$ for the homo- and heteropairs, respectively. The Tb–Tb self-quenching effects are expected to be dominant in the Tb–Tb homopair ($Tb_2\mathbf{2}(NO_3)_4{\cdot}1.2CH_3OH$), but since the Tb^{3+} ($^5D_4$) decay rate of $Tb_2\mathbf{2}(NO_3)_4{\cdot}1.2CH_3OH$ is lower than that of $(La_{0.97}Tb_{0.03})_2\mathbf{2}(NO_3)_4{\cdot}1.2CH_3OH$, concentration quenching effects are in this context unimportant. The symmetry around Tb^{3+} in the TbLa heteropairs of $(La_{0.97}Tb_{0.03})_2\mathbf{2}(NO_3)_4{\cdot}1.2CH_3OH$ is expected to be lower compared to the one found in the homodinuclear complex $Tb_2\mathbf{2}(NO_3)_4{\cdot}1.2CH_3OH$ because of the size differential between the bound La^{3+} and Tb^{3+} ions. This effect may enhance the

(31) Alpha, B.; Ballardini, R.; Balzani, V.; Lehn, J.-M.; Perathoner, S.; Sabbatini, N. *Photochem. Photobiol.* **1990**, *52*, 409.

electron transition dipole moment and hence result in a higher and temperature dependent decay rate of Tb^{3+} emission in $(La_{0.97}Tb_{0.03})_2\mathbf{2}(NO_3)_4\cdot 1.2CH_3OH$ compared to $Tb_2\mathbf{2}(NO_3)_4\cdot 1.2CH_3OH$. But changes in rates due to this effect are usually much smaller than found here.[32] Turning our attention to the possibility of Tb^{3+}-to-ligand back-energy-transfer, we find that the ligand chromophore in $La_2\mathbf{2}(NO_3)_4\cdot 1.2CH_3OH$ also decays nonexponentially with rates of 7.7×10^4 s^{-1} (early part) and 3.3×10^3 s^{-1} (tail) at room temperature and λ_{exc}= 337 nm. The ligand emission in $(La_{0.97}Tb_{0.03})_2\mathbf{2}(NO_3)_4\cdot 1.2CH_3OH$ is weak, but rates of $\approx 1.2 \times 10^5$ (early part) and 6.0×10^2 s^{-1} (tail) were estimated. The higher early time ligand decay rate of $(La_{0.97}Tb_{0.03})_2\mathbf{2}(NO_3)_4\cdot 1.2CH_3OH$ compared to that of $La_2\mathbf{2}(NO_3)_4\cdot 1.2CH_3OH$ is consistent with quenching effects of Tb^{3+} in the dilute sample, as in eq 1, where k_{LO} = the observed ligand decay rate

$$k_{LO} = k_{LC} + k_{LT} \quad (1)$$

for $(La_{0.97}Tb_{0.03})_2\mathbf{2}(NO_3)_4\cdot 1.2CH_3OH$, k_{LC} = the intrinsic cumulative decay rate of the ligand, which includes internal conversion, quenching effects within the ligand states, and spontaneous radiative and nonradiative decay rates, and k_{LT} = the ligand-to-terbium(III) energy-transfer rate.

Assuming that trapping can be abstracted from the decay rates measured in the early moments following excitation and setting $k_{LC} = 7.7 \times 10^4$ s^{-1} (the ligand decay rate in $La_2\mathbf{2}(NO_3)_4\cdot 1.2CH_3OH$) gives $k_{LT} = 4.4 \times 10^4$ s^{-1} for $k_{LO} \approx 1.2 \times 10^5$ s^{-1}. The intrinsic decay rate, $k_{LC} \approx 7.7 \times 10^4$ s^{-1}, of the short-lived luminescence of **2** in $La_2\mathbf{2}(NO_3)_4\cdot 1.2CH_3OH$ is similar to the decay rate of the short-lived Tb^{3+} emission in the complex $(La_{0.97}Tb_{0.03})_2\mathbf{2}(NO_3)_4\cdot 1.2CH_3OH$ (i.e. $k_{LC} = k_{TO} = 7.7 \times 10^4$ s^{-1}), as in eqs 1 and 2, where k_{TO} = the observed decay rate of the short-

$$k_{TO} = k_{TC} + k_{TL} \quad (2)$$

lived Tb^{3+} emission in $(La_{0.97}Tb_{0.03})_2\mathbf{2}(NO_3)_4\cdot 1.2CH_3OH$, k_{TL} = the Tb^{3+}-to-ligand back-energy-transfer rate, k_{TC} = the cumulative decay rate of the short-lived Tb^{3+} emission, which includes spontaneous radiative and nonradiative decay and other processes applicable to the $Ln_2\mathbf{2}(NO_3)_4\cdot 1.2CH_3OH$ lattice.

The parameter $k_{TC} \approx 3.6 \times 10^3$ s^{-1}, the decay rate of Tb^{3+} emission in $Tb_2\mathbf{2}(NO_3)_4\cdot 1.2CH_3OH$, provided that concentration quenching is unimportant (this is reasonable since $k_{TC} \ll k_{TO}$). This leads to $k_{TL} \approx 7.1 \times 10^4$ s^{-1}. The higher efficiency of Tb^{3+}-to-ligand back-energy-transfer suggests that the $^5D_4$ state of Tb^{3+} is probably in near resonance with the quenching ligand triplet state. The triplet absorption was not definitely observed; using that of **1** (22 200 cm^{-1}) as a reasonable estimate and the triplet emissions at 520 and 485 nm (Figure 3), we estimate the origins of the triplet states to be in the region 20 700–21 400 cm^{-1}, which is indeed very close to the $^5D_4$ state ($\approx$20 500 cm^{-1}) in $Tb_2\mathbf{2}(NO_3)_4\cdot 1.2CH_3OH$.

For the concentrated sample, $Tb_2\mathbf{2}(NO_3)_4\cdot 1.2CH_3OH$, ligand-to-$Tb^{3+}$ energy transfer is much faster due to efficient quenching by Tb^{3+} and thus ligand-Tb^{3+} electronic state equilibration does not occur. But because of the varying proximity of ligand states in $(La_{0.97}Tb_{0.03})_2\mathbf{2}(NO_3)_4\cdot 1.2CH_3OH$ to the dilute Tb^{3+} sites, a distribution of ligand emission decay rates is expected and clearly some of these states have suitable characteristics for coupling reversibly to Tb^{3+} ($^5D_4$). A summary of these energy transfer processes is shown in Figure 4.

Metal-to-ligand energy transfer was recently invoked[3,33,34] to explain the unusual luminescence decay dynamics of Eu^{3+} in $Eu_2\mathbf{1}(NO_3)_4\cdot H_2O$ and related systems.[35] Since Tb^{3+} exhibited this behavior more convincingly in this study, we investigated the

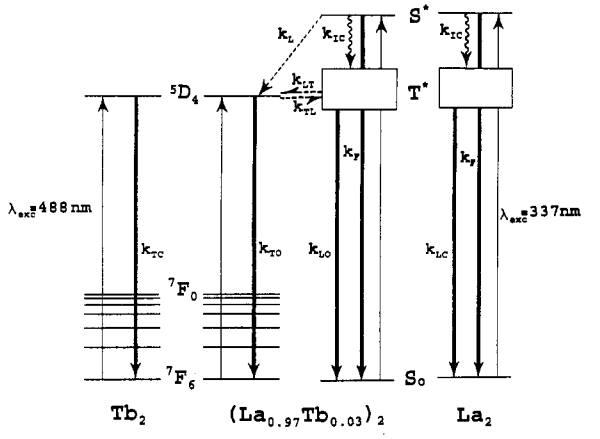

Figure 4. Summary of the essential room-temperature energy-transfer processes in the $Ln_2\mathbf{2}(NO_3)_4\cdot 1.2CH_3OH$ system: $La_2\mathbf{2}(NO_3)_4\cdot 1.2CH_3OH$ (La_2); $(La_{0.97}Tb_{0.03})_2\mathbf{2}(NO_3)_4\cdot 1.2CH_3OH$ ($(La_{0.97}Tb_{0.03})_2$); $Tb_2\mathbf{2}(NO_3)_4\cdot 1.2CH_3OH$ (Tb_2). See text for details.

dilute terbium/lanthanum sample of approximate stoichiometry[19] $(La_{0.998}Tb_{0.002})_2\mathbf{1}(NO_3)_4\cdot H_2O$. We indeed find similar behavior with Tb^{3+} emission at room temperature and λ_{exc}= 337 nm decaying at 3.3×10^5 s^{-1} and 1.4×10^5 s^{-1} for the quick and slow decay components, respectively. The ligand decay rate could not be measured using our system, but it is much higher than 10^6 s^{-1} at room temperature. At 77 K, the Tb^{3+} decay curve of $(La_{0.998}Tb_{0.002})_2\mathbf{1}(NO_3)_4\cdot H_2O$ (stoichiometry established from neutron activation analyses) shows an excitation buildup ($\approx$32 μs) and a decay rate of $\approx 9.0 \times 10^2$ s^{-1} compared to 6.2×10^2 s^{-1} for Tb^{3+} in $Ln_2\mathbf{1}(NO_3)_4\cdot H_2O$ (Ln = Tb, $Tb_{0.01}Gd_{0.99}$). The low symmetry on Tb^{3+} when coupled to La^{3+} (compared to GdTb and TbTb pairs) (vide supra) may account for this decay rate difference, but Tb^{3+}-to-ligand back-transfer at 77 K could not definitely be ruled out.[3]

Conclusion

The asymmetric lanthanide(III) cation selective dinucleating chelate **2** obtained by the relatively simple one pot synthetic protocol exhibits efficient light gathering (antenna)[8,35,36] and efficient ligand-to-Tb^{3+} exciton-transfer characteristics of practical significance to biomedical luminescent diagnostics.[3] In this context, the absence of Tb^{3+} self-quenching effects and the presence of NH groups, which can be readily converted to more efficient Ln^{3+}-binding >NR (R = CH_2COO^-, $CH_2CH_2O^-$) functionalities, are attractive qualities of chelate **2** and its Ln^{3+} complexes. The presence of functional >NH groups on chelates **2** and **3** make them potentially important sources of a variety of Ln^{3+} dinucleating macrocycles. The Tb^{3+}-to-ligand energy back-transfer observed at room temperature is unusual, and better knowledge of the phenomenon is needed in order to understand both beneficial and detrimental ligand–Ln^{3+} interaction mechanisms in photonic devices.

Acknowledgment. We thank the University of the West Indies Postgraduate and Research and Publication Committees, the British Council, the Royal Society of Chemistry, and the Third World Academy of Sciences for financial support. We also thank The Center for Nuclear Sciences, UWI, for NAA analyses and Texaco Chemicals Co. for a gift of 3,6-dioxa-1,8-octanediamine.

Supplementary Material Available: Tables of crystal data, calculated atomic positions for hydrogen atoms, complete bond distances and angles, and anisotropic displacement coefficients (7 pages). Ordering information is given on any current masthead page.

(32) Dong, W.; Flint, C. D. *J. Chem. Soc., Chem. Commun.* **1991**, 1439.
(33) Holz, R. C.; Meister, G. E.; Horrocks, W. deW., Jr. *Inorg. Chem.* **1990**, *29*, 5193.
(34) Guerriero, P.; Vigato, P. A.; Bünzli, J.-C. G.; Moret, E. J. Chem. Soc., Dalton Trans. **1990**, 647.
(35) Blasse, G. *Photochem. Photobiol.* **1990**, *52*, 417.
(36) Balzani, V.; Scandola, F. *Supramolecular Photochemistry*; Ellis Horwood Ltd.: Chichester, U.K., 1991; p 326.